Alexandria Engineering Journal (2011) **50**, 163–169

Alexandria University

Alexandria Engineering Journal

www.elsevier.com/locate/aej
www.sciencedirect.com

ORIGINAL ARTICLE

Improved flux pattern by third harmonic injection for multiphase induction machines using neural network

Ayman S. Abdel-Khalik *, Shady M. Gadoue

Department of Electrical Engineering, Alexandria University, Alexandria, Egypt

Received 2 September 2010; accepted 16 December 2010
Available online 27 August 2011

KEYWORDS

Multiphase induction machine;
Rectangular air–gap flux;
Third harmonic injection;
Eleven-phase

Abstract This paper presents a modified *V*/*f* control strategy using neural network with an improved flux pattern using third harmonic injection for multiphase induction machines. The control objective is to generate a nearly rectangular air–gap flux, resulting in an improved machine power density for the required speed range. If just a proportional relation is used between the third harmonic and fundamental plane voltage magnitudes with zero phase shift, variable misalignment between fundamental and third air–gap flux components occurs with varying mechanical loading as a result of stator voltage drop. Due to this misalignment, saturation may take place which affects the total flux and increases machine iron losses. Neural network is used to obtain the required injected voltage phasors magnitudes and angles to ensure that the air–gap flux is near rectangular with a maximum value of 1 pu for all loading conditions. Simulations are carried out on an eleven-phase induction machine to validate the proposed controller using MATLAB/Simulink.

1. Introduction

Many applications, such as electric ship propulsion, aircraft drives, locomotive traction and high power industrial plants, require high power ratings for both the motor and its converter. However, converter ratings cannot be accordingly increased due to power rating limitations of semiconductor devices [1]. A multiphase machine fed from a multiphase inverter [2] could be a suitable candidate for this task [3]. It has less current per phase or can be designed with a lower voltage for the same power. A detailed review on multiphase machines has been presented in [1]. Many references have covered various multiphase machine topics such as modeling [4,5], applications [1], performance with different control techniques [6,7], and advantages [8]. One major advantage of multiphase machines is the additional degrees of freedom offered for new applications

* Corresponding author.
E-mail address: ayman_abdelkhalik79@yahoo.com (A.S. Abdel-Khalik).

Peer review under responsibility of Faculty of Engineering, Alexandria University.
doi:10.1016/j.aej.2010.12.002

Production and hosting by Elsevier

with high torque density by current harmonic injection into concentrated machine windings [9]. Harmonic injection provides torque enhancement and can also produces more robust control [10]. Speed control strategies for multiphase induction machines are similar to those for the three-phase induction machine. Conventional constant V/f control has been employed for the multiphase variable-speed induction motor drive at steady state [11,12]. Torque enhancement at steady state was the main task of [12]. An optimization technique is used to find the suitable values for both fundamental and third harmonic flux components to obtain a near rectangular flux distribution. Consequently the magnetizing current component corresponding to each plane is calculated. Based on the steady state model, the corresponding stator voltage components are calculated. Since the conventional scalar V/f control is used, the stator voltage sequence components are assumed in phase. With mechanical loading, there is a change in the circuit impedance for each plane and the corresponding stator voltage angle changes. These assumptions yield to unequal flux tips which increases with the mechanical loading.

In this paper, a modified V/f controller is presented which gives a near flat flux pattern irrespective of mechanical loading. Neural network is used to find suitable values for both fundamental and third harmonic stator voltage space phasor components. The neural network determines the magnitude and angle of each space phasor, namely $\overline{V}_{s1}$ and $\overline{V}_{s3}$ which ensure equal flux tips at all mechanical loading levels. The required training data for the neural network are obtained from the steady state machine model in both sequence planes. The parameters of a prototype eleven-phase induction machine presented in [13] are used for the simulation study.

2. Problem description and conventional control

To obtain a nearly trapezoidal air–gap flux distribution a third harmonic component with a certain magnitude [14] is required to be in phase with the fundamental component of the air–gap flux. The desired air–gap flux distribution is shown in Fig. 1a, where both the fundamental and third harmonic space phasors are aligned. The ideal distribution has two peaks of 1 pu at 60° and 120° [14]. The V/f controller employed in [12] applies in phase stator voltage sequence components to the machine stator terminals. Due to the stator voltage drop, which is different in both fundamental and third plane, the corresponding induced EMF sequence components are not completely aligned. At no-load, the stator voltage drop may be neglected which yields approximately aligned air–gap flux components. However, as the machine is loaded the stator voltage drop results in unequal flux tips caused by the misalignment of the two components of the induced EMF space phasor. Fig. 1b illustrates this case assuming a 10° misalignment between the two space phasors due to a certain mechanical loading. It is shown that the first peak at 60° exceeds 1 pu and the second peak is less than 1 pu. If saturation is not considered, there is no effect since the two curves have the same area; hence, the total flux is not affected. However, if saturation occurs, the total flux and saturation will increase the machine iron losses. The severity of this problem will be dependent on the stator voltage drop which is different depending on the machine rating.

To overcome this problem the angle between the two components of the applied stator voltage components should be selected variable, not zero as in [12], to ensure aligned components of the internally induced EMF. In this paper, the steady state model is used to find the required phase angle of the two components of the applied stator voltage for different loading conditions.

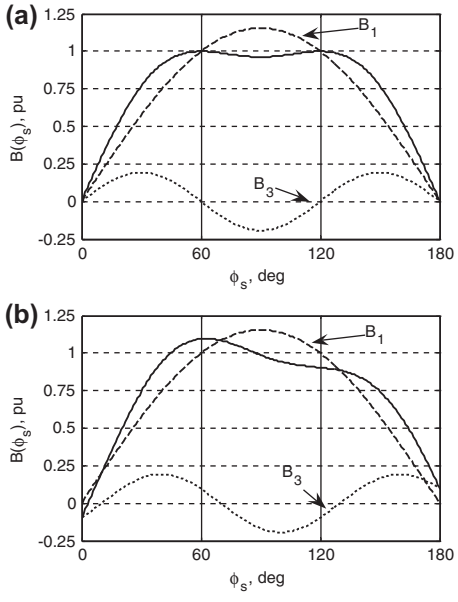

Figure 1 Flux density distribution and its components (a) aligned and (b) misaligned.

3. Steady state model

The multiphase machine steady state model and the equivalent circuit for any sequence k, shown in Fig. 2, are given in [13].

To maintain a quasi-trapezoidal air–gap flux density distribution, the optimum air–gap flux distribution, for maximum fundamental air–gap flux density, is given in pu by [13,14]

$$B(\phi_s) = B_1(\sin\phi_s + k_3 \sin 3\phi_s) \tag{1}$$

where

$$B_1 = 1.15\ \text{pu}, \quad k_3 = \frac{1}{6}$$

and ϕ_s is the stator periphery angle.

This flux density induces a voltage with the same waveform shape and can be composed from two components E_{m1} and E_{m3}, which represents the internal induced voltages in both sequence circuits.

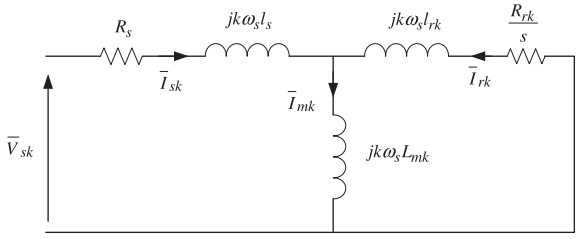

Figure 2 Steady-state equivalent circuit for any sequence k.

It is required that the two components of the internal EMF are aligned for all loading conditions. This can be done by first defining E_{m1} and E_{m3} as:

$$\overline{E}_{m1} = (V/f \text{ Ratio}) \times 1.15 \times f\angle 0 \tag{2}$$

$$\overline{E}_{m3} = \overline{E}_{m1} \times \frac{1}{6} \tag{3}$$

The corresponding magnetizing currents I_{m1} and I_{m3} are given by:

$$\overline{I}_{m1} = -j\frac{E_{m1}}{\omega_s L_{m1}} \tag{4}$$

and

$$\overline{I}_{m3} = \frac{E_{m3}}{3\omega_s L_{m3}} = \frac{k_3 E_{m1}}{3\omega_s L_{m3}} = \frac{k_3 L_{m1}}{3L_{m3}} I_{m1} \tag{5}$$

where L_{m1} and L_{m3} are the magnetizing inductances for the fundamental and third planes, respectively, and ω_s is angular frequency.

The machine reactances for the fundamental and 3rd harmonic at each frequency are given by:

$$X_{s1} = \omega_s \cdot l_s; \quad X_{r1} = \omega_s \cdot l_{r1}; \quad X_{m1} = \omega_s \cdot L_{m1} \tag{6}$$

$$X_{s3} = 3\omega_s \cdot l_s; \quad X_{r3} = 3\omega_s \cdot l_{r3}; \quad X_{m3} = 3\omega_s \cdot L_{m3} \tag{7}$$

where l_s is the stator leakage inductance, l_{r1} and l_{r3} are the rotor leakage inductances for the fundamental and third planes, respectively.

The corresponding rotor current components for both planes can be given by:

$$\overline{I}_{r1} = \frac{\overline{E}_{m1}}{R_{r1}/s + jX_{r1}}, \quad \overline{I}_{r3} = \frac{\overline{E}_{m3}}{R_{r3}/s + jX_{r3}} \tag{8}$$

where R_{r1} and R_{r3} are the rotor resistances for the fundamental and third planes, respectively, and s is the machine slip.

The stator current components are then calculated from:

$$\overline{I}_{s1} = \overline{I}_{m1} + \overline{I}_{r1}, \quad \overline{I}_{s3} = \overline{I}_{m3} + \overline{I}_{r3} \tag{9}$$

The magnitude of the total stator RMS current is given by:

$$I_{mt} = \sqrt{|\overline{I}_{s1}|^2 + |\overline{I}_{s3}|^2} \tag{10}$$

Hence, the fundamental and third harmonic stator voltages can be calculated as:

$$\overline{V}_{s1} = \overline{E}_{m1} + \overline{I}_{s1}(R_s + jX_{s1}) \tag{11}$$

$$\overline{V}_{s3} = \overline{E}_{m3} + \overline{I}_{s3}(R_s + jX_{s3}) \tag{12}$$

Fig. 3 illustrates the phasor diagram representing the relation between different machine variables for both planes. At no-load the angles δ_1 and δ_3 are approximately equal. However, as the machine is loaded these two angles will not be equal.

The machine developed torque can be calculated as:

$$T_e = \frac{np}{\omega_s}\left(|\overline{I}_{r1}|^2 \frac{R_{r1}}{s} + |\overline{I}_{r3}|^2 \frac{R_{r3}}{s}\right) \tag{13}$$

where n is the number of phases and p is the number of pole pairs.

Contour charts, given in Figs. 4 and 5, are plotted for both fundamental and third sequence planes. These charts can be used to determine the required stator voltage magnitude and angle for both planes as a function of the input frequency

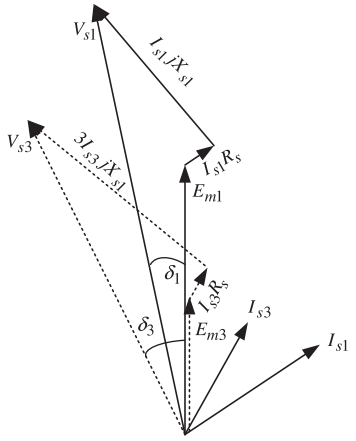

Figure 3 Phasor diagram of the multi-phase machine with third harmonic injection.

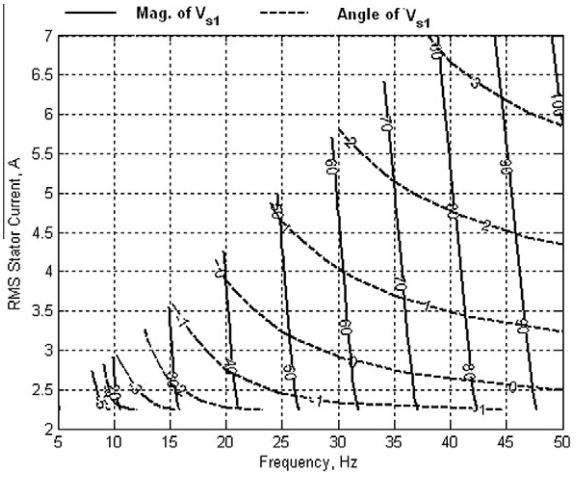

Figure 4 Contour chart for the fundamental component of the stator voltage phasor.

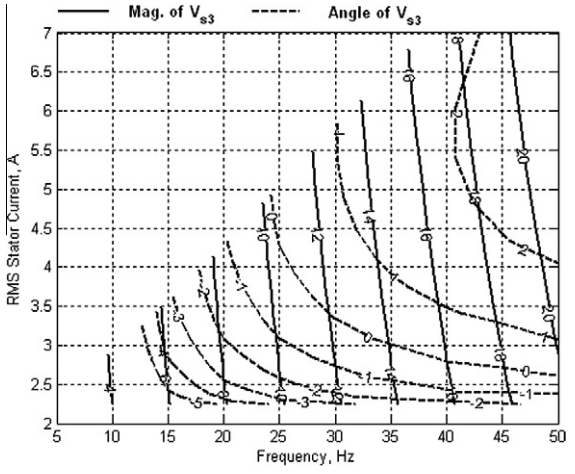

Figure 5 Contour chart for the third harmonic component of the stator voltage phasor.

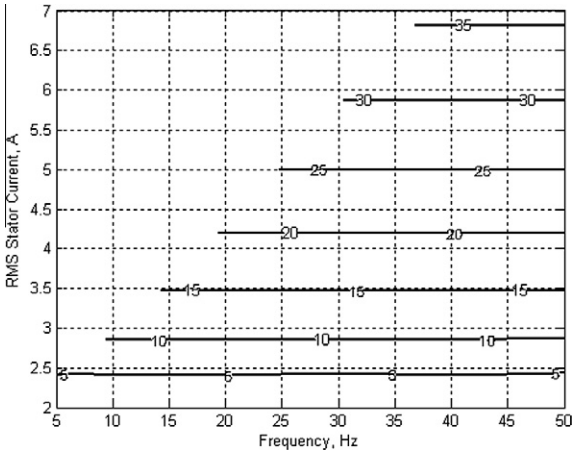

Figure 6 Contour chart for the machine developed torque.

and the total RMS stator current. It is evident that, for a given frequency, the required voltage magnitude for both planes increases as the machine stator current increases with mechanical loading to compensate for the stator voltage drop. The angles of the two stator voltage components are approximately equal for light loads. However, the difference between them increases as the machine is mechanically loaded. Fig. 6 illustrates the contour chart for the machine developed torque. It can be shown that the machine developed torque for a given stator current is constant irrespective of the applied frequency.

4. Neural network modified *V*/*f* control

Artificial intelligence techniques, especially NNs, have gained much interest over the past few years. Artificial NNs are based on the basic model of the human brain with capability of generalization and learning. They are frequently used as universal nonlinear function approximators to represent functions with weighted sums of nonlinear terms [15]. Multilayer feedforward NNs have shown a great capability to model complex nonlinear systems. The advantages of applying NNs include fault tolerance, parallel processing, fast implementation speed, noise-immunity, and generalization capability. However, lack of design techniques and computational effort requirement are the main drawbacks of NNs. A comprehensive review of applications of NN in the field of power electronics and motor drives is covered in [16].

To improve the flux distribution at all loading conditions a NN is proposed here to control not only the magnitudes of V_{s1} and V_{s3} as in [12] but also the phase angles of these voltages δ_1 and δ_3. Hence a multilayer feedforward NN is employed to generate these values from the command frequency and the magnitude of the total stator current. These two inputs are chosen to represent the operating speed and the load level applied to the motor. The outputs from the NN are the magnitudes of V_{s1} and V_{s3} and their phase angles δ_1 and δ_3. Hence an 2-20-4 NN controller is used where the number of neurons in the hidden layer is chosen by a trial and error technique. Hyperbolic tan (tan-sigmoid) and linear activation functions are used in the hidden and output layers, respectively. The structure of the proposed NN is shown in Fig. 7.

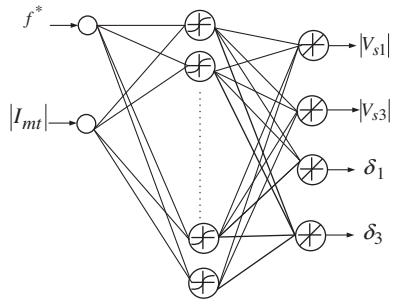

Figure 7 Neural network architecture.

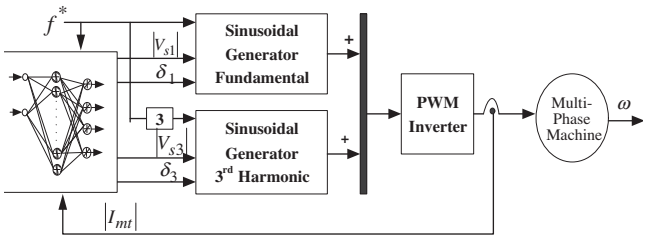

Figure 8 Proposed control scheme.

The steady state equations given in the previous section are used to generate the training data for the NN for a frequency range of 5–50 Hz and a slip range of 0–0.1. At each point the voltages magnitudes and corresponding phase angles required to make E_{m1} and E_{m3} in phase are calculated. Hence a 100 input/output pattern is obtained and is used to train the proposed NN. The training is performed off-line with MATLAB/Simulink using the Levenberg–Marquardt training algorithm which is faster than the gradient descent back propagation algorithm but needs a large memory. The training stops when the Mean Squared Error (MSE) between targets and neural network outputs decays to a satisfactory level of (1×10^{-5}) after about 2500 epochs. Once trained, the NN gives a fast execution speed due to its parallel processing. The proposed control scheme using NN is shown in Fig. 8.

5. Simulation results

In the following cases, the proposed control scheme is simulated using the machine transient dq model, given in [4,13], to check the validity of the proposed controller. The simulation is carried out using MATLAB/Simulink.

5.1. Effect of mechanical loading

In this case, the supply frequency is set to its rated value, namely 50 Hz, and the machine is accelerated mechanically unloaded to its no-load speed, approximately 1500 rpm. After 1 s the machine is loaded with its full load torque, 16 N m. The machine speed and its developed torque are shown in Figs. 9 and 10 while the machine stator phase current is shown in Fig. 11. The internal induced EMF and the corresponding magnetizing current are shown in per unit in Fig. 12 with the

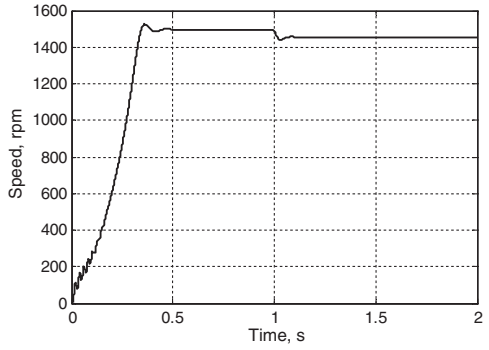

Figure 9 Machine speed.

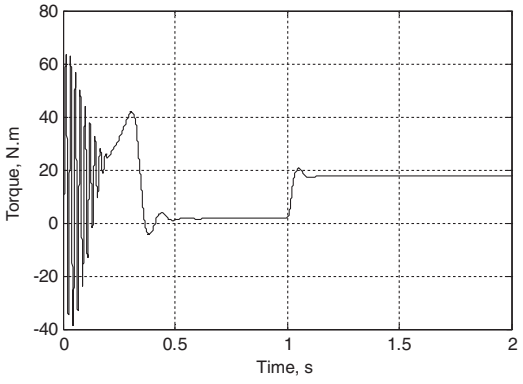

Figure 10 Machine developed torque.

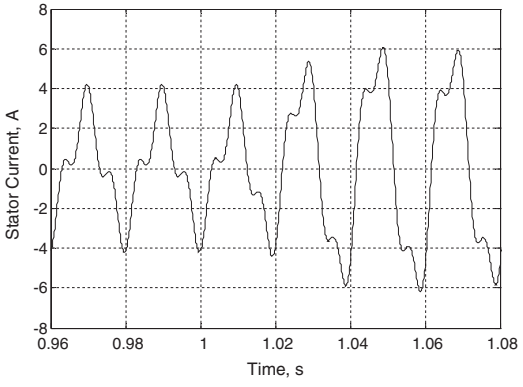

Figure 11 Machine stator phase current.

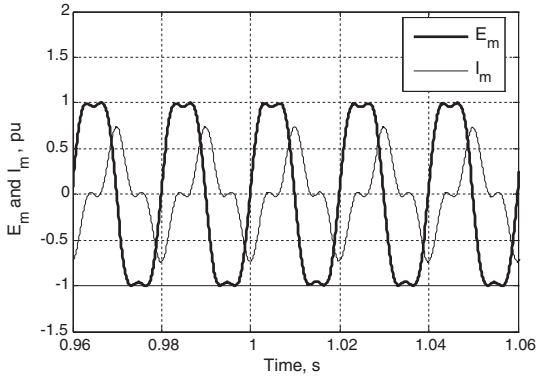

Figure 12 Internal induced EMF and the corresponding magnetizing current.

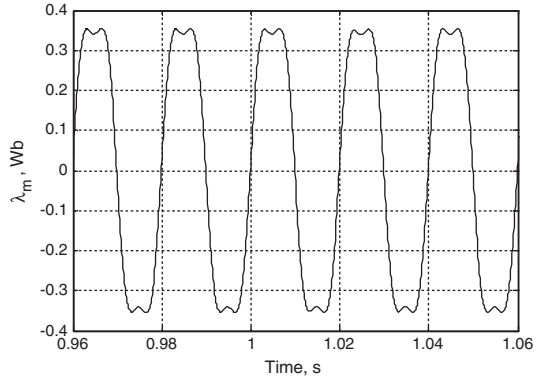

Figure 13 Air–gap flux linkage.

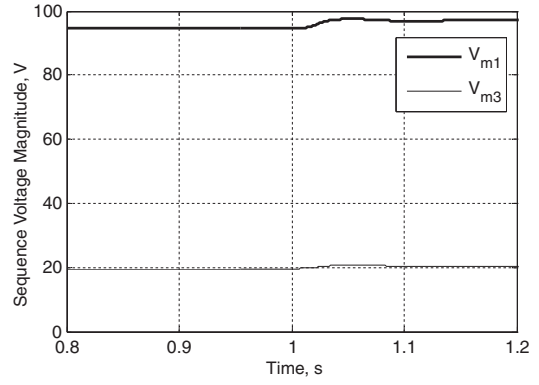

Figure 14 Stator voltage sequence components magnitude.

magnetizing flux linkage shown in Fig. 13. It is evident that the flux linkage including its two tips is not affected by the mechanical loading. The neural network outputs, namely sequence voltages magnitudes and angles, are shown in Figs. 14 and 15, respectively. It is shown that the magnitude of both components of the stator voltage increases as the machine is mechanically loaded to compensate for the stator voltage drop as mentioned before. Moreover, the difference angle between the two components of the stator voltage space phasor is also changed to ensure aligned components of the internal EMF.

5.2. Machine acceleration

In this case, the supply frequency is increased linearly from 20 Hz, which gives a synchronous speed of 600 rpm, to 50 Hz, which gives the rated synchronous speed of 1500 rpm. The machine speed variation and the corresponding developed torque are shown in Figs. 16 and 17, respectively. The magnetizing flux linkage is shown in Fig 18. It is shown that the flux magnitude is constant during the whole acceleration period

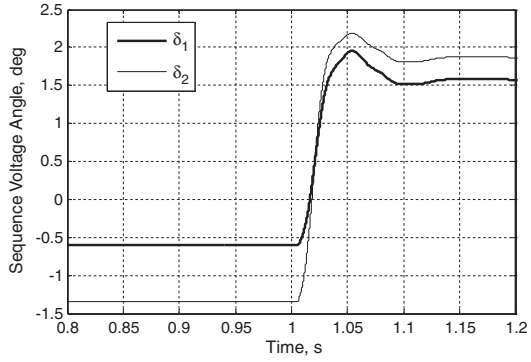

Figure 15 Stator voltage sequence components angle.

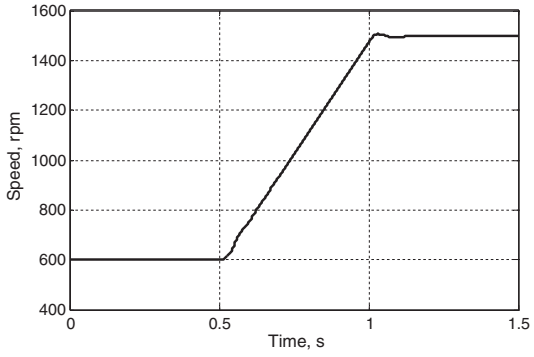

Figure 16 Machine speed with ramp acceleration.

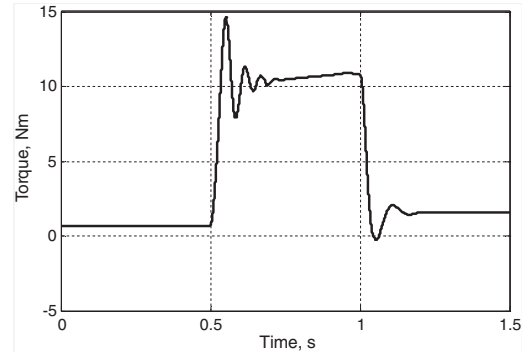

Figure 17 Machine developed torque for ramp acceleration.

while its frequency increases as the machine speed increases. It is also shown that the waveform tips are constant irrespective of the machine speed. This case proves the validity of the proposed controller for the given frequency range.

6. Conclusion

This paper has presented a NN-based modified V/f control strategy for multi-phase induction motor. The basic concept is to control both magnitudes and phase angles of the fundamental and third harmonic injected voltages to ensure optimal flux distribution at different mechanical loading conditions. A multi-layer feedforward NN controller is proposed here to generate the magnitude and phase of the two components of the stator voltage space vector. The NN inputs are the command frequency and the total RMS stator current magnitude. The stator current input is used to compensate for the stator voltage drop for different mechanical loads to ensure aligned components of the internal air–gap flux. The training data of the NN are obtained from the machine steady state equivalent circuit. The proposed control scheme is tested using MATLAB/Simulink and results show constant flux magnitude with equal flux tips at different loading conditions.

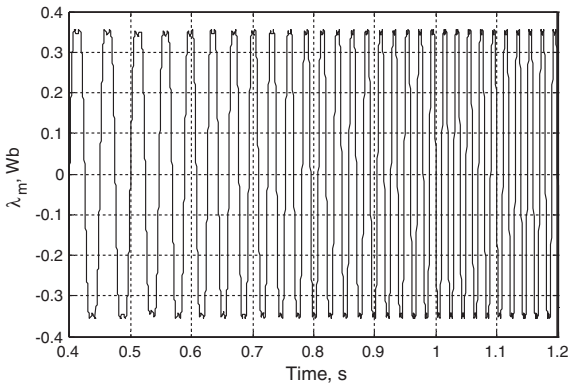

Figure 18 Machine air–gap flux linkage during ramp acceleration.

Appendix

Machine ratings		
Rated power	hp	3
Synchronous speed	rpm	1500
No. of poles		4
Phase voltage	V	82
Rated phase current	A	4
Supply frequency	Hz	50
No. of phases		11
Phase connections		Star
No. of stator slots		44
Rotor radius	mm	63
Rotor stack length	mm	121
No. of rotor slots		28
Number of turns per stator phase		80

Machine parameters referred to the stator					
R_s	0.74 Ω	l_s	5.3 mH		
R_{r1}	1	l_{r1}	16 mH	L_{m1}	140.3 mH
R_{r3}	1.3351	l_{r3}	21.36 mH	L_{m3}	17.97 mH

References

[1] E. Levi, Multiphase electric machines for variable-speed applications, IEEE Transactions on Industrial Electronics 55 (5) (2008) 1893–1909.

[2] D. Dujic, M. Jones, E. Levi, Analysis of output current ripple rms in multiphase drives using space vector approach, IEEE Transactions on Power Electronics 24 (8) (2009) 1926–1938.

[3] E. Levi, R. Bojoi, F. Profumo, H.A. Toliyat, S. Williamson, Multiphase induction motor drives – a technology status review, IET Electric Power Applications 1 (4) (2007) 489–516.
[4] L.A. Pereira, C.C. Scharlau, L.F.A. Pereira, J.F. Haffner, General model of a five-phase induction machine allowing for harmonics in the air–gap field, IEEE Transactions on Energy Conversion 21 (4) (2006) 891–899.
[5] M. Jones, S.N. Vukosavic, E. Levi, Parallel-connected multiphase multi-drive systems with single inverter supply, IEEE Transactions on Industrial Electronics 56 (6) (2009) 2047–2057.
[6] Z. Libo, J.E. Fletcher, B.W. Williams, H. Xiangning, Dual-plane vector control of a five-phase induction machine for an improved flux pattern, IEEE Transactions on Industrial Electronics 55 (5) (2008) 1996–2005.
[7] A. Yong-Le, M.J. Kamper, A.D. Roux, Novel direct flux and direct torque control of six-phase induction machine with nearly square air–gap flux density, IEEE Transactions on Industry Applications 43 (6) (2007) 1534–1543.
[8] H.A. Toliyat, Analysis and simulation of five-phase variable-speed induction motor drives under asymmetrical connections, IEEE Transactions on Power Electronics 13 (4) (1998) 748–756.
[9] H.A. Toliyat, T.A. Lipo, J.C. White, Analysis of a concentrated winding induction machine for adjustable speed drive applications. II. Motor design and performance, IEEE Transactions on Energy Conversion 6 (4) (1991) 684–692.
[10] M.J. Duran, F. Salas, M.R. Arahal, Bifurcation analysis of five-phase induction motor drives with third harmonic injection, IEEE Transactions on Industrial Electronics 55 (5) (2008) 2006–2014.
[11] K.N. Pavithran, R. Parimelalagan, R. Krishnamurthy, M.R. Studies, On inverter-fed five-phase induction motor drive, IEEE Transactions on Power Electronics 3 (2) (1988) 224–235.
[12] C.C. Scharlau, L.F.A. Pereira, L.A. Pereira, S. Haffner, Performance of a five-phase induction machine with optimized air–gap field under open loop V/f control, IEEE Transactions on Energy Conversion 23 (4) (2008) 1046–1056.
[13] A.S. Abdel-khalik, M.I. Masoud, B.W. Williams, Eleven phase induction machine: steady-state analysis and performance evaluation with harmonic injection, IET Electric Power Applications 4 (8) (2010) 670–685.
[14] R.O.C. Lyra, T.A. Lipo, Torque density improvement in a six-phase induction motor with third harmonic current injection, IEEE Transactions on Industry Applications 38 (5) (2002) 351–1360.
[15] P. Vas, Artificial-Intelligence-based Electrical Machines and Drives—Application of Fuzzy, Neural, Fuzzy-Neural and Genetic Algorithm based Techniques, Oxford University Press, New York, 1999.
[16] B.K. Bose, Neural network applications in power electronics and motor drives—an introduction and perspective, IEEE Transactions on Industrial Electronics 54 (1) (2007) 14–33.